Invest Ophthalmol Vis Sci. Author manuscript; available in PMC 2014 March 09.

Published in final edited form as:
Invest Ophthalmol Vis Sci. 2010 February ; 51(2): 1151–1163. doi:10.1167/iovs.09-3622.

Microarray Analysis Identifies Changes in Inflammatory Gene Expression in Response to Amyloid-β Stimulation of Cultured Human Retinal Pigment Epithelial Cells

Khaliq H. Kurji[1,2], **Jing Z. Cui**[1,2], **Tony Lin**[1], **David Harriman**[1], **Shiv S. Prasad**[3], **Ljuba Kojic**[1,2], and **Joanne A. Matsubara**[1,2]

[1]Department of Ophthalmology and Visual Sciences, University of British Columbia, Vancouver, British Columbia, Canada

[2]Brain Research Centre, University of British Columbia, Vancouver, British Columbia, Canada

[3]Centre for Biologics Research, Biologics and Genetic Therapies Directorate, Health Canada, Ottawa, Ontario, Canada

Abstract

Purpose—Age-related macular degeneration (AMD) is a common cause of irreversible vision loss in the elderly. The hypothesis was that in vitro stimulation of RPE cells with A$\beta_{1\text{-}40}$, a constituent of drusen, promotes changes in gene expression and cellular pathways associated with the pathogenesis of AMD, including oxidative stress, inflammation, and angiogenesis.

Methods—Confluent human RPE cells were stimulated with A$\beta_{1\text{-}40}$, or the reverse peptide A$\beta_{40\text{-}1}$, and genome wide changes in gene expression were studied with gene microarrays. Selected genes were verified by qRT-PCR and ELISA. Pathway analysis with gene set enrichment analysis (GSEA) and ingenuity revealed top functional pathways in RPE after A$\beta_{1\text{-}40}$ stimulation.

Results—RPE cells stimulated with A$\beta_{1\text{-}40}$ (0.3 μM) for 24 hours resulted in 63 upregulated and 22 downregulated previously known genes. The upregulated genes were predominantly in inflammatory and immune response categories, but other categories were also represented, including apoptosis, cell signaling, cell proliferation, and signal transduction. Categories of downregulated genes included immune response, transporters, metabolic functions and transcription factors. ELISA confirmed that secreted levels of *IL-8* were two times higher than control levels. GSEA and ingenuity analysis confirmed that the top affected pathways in RPE cells after A$\beta_{1\text{-}40}$ stimulation were inflammation and immune response related. Surprisingly, few angiogenic pathways were activated at the doses and exposure times studied.

Conclusions—A$\beta_{1\text{-}40}$ promotes RPE gene expression changes in pathways associated with immune response, inflammation, and cytokine and interferon signaling pathways. Results may relate to in vivo mechanisms associated with the pathogenesis of AMD.

Corresponding author: Joanne A. Matsubara, Department of Ophthalmology and Visual Sciences, University of British Columbia, Vancouver, BC V5Z 3N9, Canada; jms@interchange.ubc.ca.

Disclosure: **K.H. Kurji**, None; **J.Z. Cui**, None; **T. Lin**, None; **D. Harriman**, None; **S.S. Prasad**, None; **L. Kojic**, None; **J.A. Matsubara**, None

Age-related macular degeneration (AMD) is the most common cause of irreversible vision loss in the elderly. The disease is characterized by extracellular deposits known as drusen, which are found between the basal lamina of the retinal pigment epithelium (RPE) and the inner layer of Bruch's membrane (BM). Although, the presence of drusen correlates with the development of AMD, the specific mechanisms underlying the biogenesis of drusen and its relationship to the disease remain elusive.[1–3] Extensive biochemical analysis of drusen revealed the presence of several proteins linked to inflammation. Such proteins include immunoglobulins, acute-phase molecules (vitronectin, amyloid P, and fibrinogen), complement factors (*C5* and *C5b-9*), and complement regulatory molecules (clusterin and complement receptor 1).[4–8] These findings implicate an inflammatory process associated with drusen, but what activates or triggers the inflammation remains unknown.[4,9–12]

Several lines of evidence suggest that amyloid-$\beta_{1\text{-}40}$ (A$\beta_{1\text{-}40}$), a known constituent of drusen, is a potential candidate trigger peptide.[3,13–15] Genetically modified mice with increased Aβ deposition display many traits consistent with human AMD, such as the accumulation of sub-RPE deposits, microglial activation, and degeneration of the retinal neurons and RPE.[16,17] In the retina, cell types including neurons, RPE, and glia may provide a local source of Aβ species; they have been shown to have the cellular machinery for the synthesis of amyloid precursor protein (*APP*) and cleavage enzymes.[10] Sequential *APP* processing by β- and γ-secretase produces the major Aβ species, A$\beta_{1\text{-}40}$. Recent in vitro studies in which RPE cells are stimulated with A$\beta_{1\text{-}40}$ demonstrated several results that are consistent with a proinflammatory response. Wang et al.[18] reported that A$\beta_{1\text{-}40}$ stimulation caused abnormal activity of complement factor I (*CFI*), an inhibitory regulator of the complement cascade. In another study, stimulation of RPE cells with A$\beta_{1\text{-}40}$ modulated the expression of vascular endothelial growth factor (*VEGF*), which is known to promote angiogenesis, a late-stage feature of AMD.[17] These results prompted us to further elucidate the effects of A$\beta_{1\text{-}40}$ stimulation on RPE cells in vitro by differential microarrays and corresponding functional pathway analysis. We hypothesize that A$\beta_{1\text{-}40}$ stimulation of RPE cells in vitro promotes gene expression changes associated with cellular pathways implicated in the pathogenesis of AMD, including oxidative stress, inflammation, angiogenesis, and apoptosis.

Methods

A$\beta_{1\text{-}40}$ Oligomerization

We chose to focus on the effects of the oligomeric form of A$\beta_{1\text{-}40}$ because, unlike A$\beta_{1\text{-}42}$ (the more toxic form associated with Alzheimer's plaques), A$\beta_{1\text{-}40}$ was identified in drusen sites.[3] Also, a recent study[19] using an RPE cell line compared oligomeric A$\beta_{1\text{-}40}$ with A$\beta_{1\text{-}42}$ and demonstrated that their effects on RPE function were comparable, confirming original reports by Kayed et al.[20] that A$\beta_{1\text{-}40}$ and A$\beta_{1\text{-}42}$ have similar toxic effects on several cell types tested.

A$\beta_{1\text{-}40}$ peptide and the control reverse peptide A$\beta_{40\text{-}1}$ were purchased from American Peptide (Sunnyvale, CA) as a salt-free, lyophilized powder. The protocol used to synthesize Aβ oligomers was obtained from Invitrogen Canada (Burlington, ON, Canada). Briefly, lyophilized A$\beta_{1\text{-}40}$ (or the reverse peptide A$\beta_{40\text{-}1}$) was dissolved in 200 μL

hexafluoroisopropanol (HFIP) and sonicated for 30 seconds. The HFIP solution was then transferred by a 22-gauge syringe to a new 1.4-mL tube (Eppendorf, Fremont, CA) containing 700 μL of distilled water. A Teflon-coated micromagnetic stirring bar was added, and the tube was closed with a perforated cap to allow HFIP to vent after evaporation. The tube was placed in a holder inside a fume hood on top of a stirring plate, and stirred with a Teflon-coated micro stir bar at 300 rpm for 24 to 48 hours. Aliquots of the supernatant were analyzed for confirmation of Aβ oligomers using atomic force microscopy (AFM) and dot blot assay.

Atomic Force Microscopy

AFM was performed as previously described.[21,22] Briefly, $A\beta_{1\text{-}40}$ samples were prepared for AFM examination by placing 10 μL of solution onto freshly cleaved mica (Ted Pella, Inc., Redding, CA). The sample was allowed to adhere to the mica surface for 10 minutes at room temperature and was subsequently washed with double-distilled water to eliminate contamination due to buffer and salts and to help reduce background contrast. AFM images were captured with a microscope (BioScope with the Nanoscope IIIa Controller and a G-type scanner; Digital Instruments, Santa Barbara, CA). The contact mode was used for all images with DNP silicon nitride cantilevers (Digital Instruments). A minimum of four random regions of the mica surface was examined to ensure that similar structures existed throughout the sample.

Dot Blot Assay

A dot blot assay was performed to determine the oligomeric form $A\beta_{1\text{-}40}$. Approximately 3 μL of $A\beta_{1\text{-}40}$ solution was spotted onto a nitrocellulose membrane and allowed to dry. The membrane was then blocked with 10% nonfat dry milk in Tris-buffered saline (TBS) containing 0.01% Tween 20 (TBST) solution overnight at 4°C, and washed three times in full-strength TBST for 5 minutes before being incubated for 1 hour at room temperature with the A11 anti-oligomer antibody using the manufacturer's protocol (Invitrogen Corp., Carlsbad, CA). The membrane was then washed three times in TBST for 5 minutes and incubated for 1 hour at room temperature with a standard horseradish peroxidase–conjugated secondary antibody made in goat against rabbit IgG diluted at 1:2000 (Promega, Madison, WI). The blots were finally washed three times in TBST for 5 minutes and developed for 20 minutes in a solution of tetramethylbenzidine (TMB; Promega).

Cell Culture of Human RPE Cells

Human fetal RPE cells were used in all the experiments. Human RPE cells were isolated from fetal donor eye tissues, as described elsewhere.[23,24] Methods for securing human tissue were humane and included proper written informed consent, which complied with the Declaration of Helsinki. Human fetal donor eyes had no known disease and were used under the guidelines and regulation of the IRB at the University of British Columbia, Vancouver, Canada. The eyes were cut circumferentially, the vitreous removed, and the neuroretina gently detached from the RPE cell layer. The choroid/RPE layer was placed in 2% Dispase (Invitrogen) in Hanks' balanced salt solution (HBSS; Invitrogen) for 25 minutes at 37°C. The RPE layer was then removed in fragments and passed through 70- and 40-μm nylon mesh filters (Falcon Plastics, Oxnard, CA). Only the fragments that were left behind were

retained. After centrifugation at 1500 rpm for 5 minutes, the fragments were gently dissociated and seeded on to laminin-coated six-well plates (Falcon Plastics). RPE cells were cultured in Dulbecco's modified Eagle's medium (DMEM; Invitrogen-Gibco, Grand Island, NY) containing 10% fetal bovine serum (FBS; Invitrogen-Gibco), 100 μg/mL penicillin (Sigma-Aldrich, St. Louis, MO), 100 μg/mL streptomycin (Sigma-Aldrich), and 2 mM L-glutamine (Invitrogen) at 37°C in a humidified atmosphere of 95% air and 5% CO_2. At confluence, the cells were detached with 0.05% trypsin/0.02% EDTA (Invitrogen), collected by centrifugation, and expanded. In the following experiments, passage 5 cells were used, and RPE cells from the same donor were used in an individual experiment.

Cell Viability Assay

RPE cells (20×10^3 cells/well) were seeded in 200 μL medium on a 96-well culture plate and incubated with DMEM containing 10% FBS, for 24 hours. The medium was then discarded, and the cells were washed three times with phosphate-buffered saline (PBS). The MTT reduction assay was used as an index of cell viability. Briefly, the oligomeric form of A$\beta_{1\text{-}40}$ (0.01, 0.3, 1.0, 5.0, and 10.0 μM) and the control, reverse peptide, A$\beta_{40\text{-}1}$ (0.3 μM) were used to stimulate RPE cells for various lengths of time (3, 6, 12, or 24 hours). After stimulation, the media were aspirated and the RPE cells were subsequently incubated in serum-free medium containing 0.4 mg/mL MTT [3-(4,5-dimethylthiazol-2-yl)-2,5-diphenyltetrazolium bromide] for 4 hours. Mitochondrial and cytosolic dehydrogenases of living cells reduced the yellow tetrazolium salt (MTT) to a purple formosan dye that was then detected by spectrophotometry. After 4 hours, the MTT solution was aspirated, and 150 μL of dimethylsulfoxide (DMSO) was added for a period of 20 minutes. Optical densities of the supernatant were read at 550 nm with a microplate spectrophotometer (Bio-Tek Instruments, Inc., Winooski, VT). Absorbances were normalized to those of the untreated control cultures, which were also incubated in serum-free medium, which represented 100% viability. Two independent experiments in quadruplicate were performed in this study. The mean ± SD of the data was analyzed.

Aβ Stimulation

RPE cells (0.3×10^6/well) were seeded in 2 mL of culture medium in a six-well plate for 4 days. Before stimulation, the cells were washed three times with PBS. The RPE cells were then treated with A$\beta_{1\text{-}40}$ (the oligomeric form) or A$\beta_{40\text{-}1}$ (the reverse peptide) at a concentration of 0.3 μM for 3, 6, 12, or 24 hours in 1 mL of serum-free DMEM. Untreated RPE cells containing only serum-free DMEM were used as the negative control. As the chemical constituents of serum often vary, serum-free DMEM was used in all stimulation studies to ensure a controlled experimental design.

Microarray and Data Analysis

The total cellular RNA was isolated from cultured human RPE cells according to manufacturer's recommendations (TRIzol; Invitrogen). RNA samples were then subsequently treated with DNase treatment and removal (TURBO DNA-free; Ambion, Streetsville, ON, Canada). Quantification of RNA was performed with spectrophotometry (ND-1000; NanoDrop Products, Thermo Fisher Scientific, Wilmington, DE). Total RNA

integrity was confirmed with a bioanalyzer (model 2100; Agilent Technologies, Palo Alto, CA) according to the manufacturer's protocol.

The labeling and hybridization of the cRNA was performed at the Prostate Cancer Microarray Centre, University of British Columbia. One microgram of total RNA from all samples and from human universal reference RNA (Stratagene, La Jolla, CA) was amplified and labeled with fluorescent dyes (Cy3 and Cy5; Low RNA Input Linear Amplification Labeling Kit; Agilent Technologies) according to the manufacturer's protocol. The amount and specific activity of the resulting fluorescently labeled cDNA was assessed with the spectrophotometer. Equal amounts of Cy3- sample and Cy5-labeled universal human reference cDNA were cohybridized (Whole Human Genome Oligo Microarray; Agilent Technologies), comprising over 41,000 human genes and transcripts, for 18 hours before washing and scanning. Data were extracted from the resulting images (Feature Extraction Software; Agilent Technologies).

Red (Cy5 labeled cRNA) and green (Cy3 labeled cRNA) processed signals were entered into the computer software (GeneSpring 7.3.1; Agilent Technologies) and normalized via manufacturer's protocols for two-color experiments as follows: per spot, divide by control channel; per chip, normalize to the 50th percentile; per gene, normalized to median. The results represent the mean values from three independent experiments. A list of differentially expressed genes was generated by applying a *t*-test with $P < 0.05$ between the A$\beta_{1\text{-}40}$-treated group and the untreated group and by applying a change filter with a cutoff of ±1.5-fold. Linearization of the data was undertaken by $\log_2$ transformation.

Real-Time Quantitative (q)RT-PCR

Reverse transcription reactions were performed for each RNA sample (1 μg) using reverse transcription reagents (Superscript III; Invitrogen Canada). Real-time PCR was performed with a sequence-detection system (Prism 7300; Applied Biosystems [ABI], Foster City, CA). SYBR green PCR master mix (ABI) was used on cDNA samples in 96-well optical plates and analyzed by using qRT-PCR methods, as described elsewhere.[25] Oligonucleotide primers for all genes of interest and for the housekeeping gene glyceraldehyde-3-phosphate dehydrogenase (*GAPDH*) were designed for real-time PCR on computer (Primer Express 2.0 software; ABI). All primers were purchased from Proligo LL (Boulder, CO). Relative quantification of gene expression was performed using the *x*-fold change method, as published[26] and as recommended by the manufacturer of the sequence detection system (ABI). The relative gene expression was represented by the difference between the normalized values of the experimental samples to that of corresponding sham controls (ΔΔCt). $2^{-\Delta\Delta Ct}$ for each product was used to calculate changes. A Pearson's correlation coefficient was used to calculate the correlation between microarray and qRT-PCR $\log_2$-fold changes.

ELISA

Levels of *IL-1β*, *Il-8*, and tumor necrosis factor (*TNF*)–related apoptosis-inducing ligand TNFSF10 (*TRAIL*) in the supernatant samples were measured using proteome arrays (SearchLight; Thermo Fisher Scientific, Woburn, MA). Samples were incubated for 1 hour

on the array plates that were prespotted with capture antibodies specific for each protein biomarker. The plates were emptied and washed three times before the addition of a cocktail of biotinylated detection antibodies to each well and then were incubated for 30 minutes. The plates were then washed three times and incubated again for 30 minutes with streptavidin-horseradish peroxidase. All incubations were at a room temperature with agitation at 200 rpm. The plates were again washed before the addition of chemiluminescent substrate (SuperSignal Femto; Thermo Fisher Scientific) and were immediately imaged (SearchLight; Thermo Fisher Scientific) and the data analyzed (Array Analyst software; Ambion).

Gene Set Enrichment Analysis (GSEA)

To test for sets of related genes that might be systematically altered in A$\beta_{1\text{-}40}$-treated RPE cells, we performed studies of gene sets in functional pathways by analyzing our microarray dataset using GSEA.[27] A total of 1892 curated gene sets containing genes whose products are involved in specific metabolic and signaling pathways were obtained from pathway databases or from peer-reviewed published material. The gene sets were screened against the GSEA-ranked microarray data sets to calculate enrichment score (ES) for each gene set. An enrichment score reflects the degree to which a gene set is overrepresented at the extreme top or bottom of the ranked microarray data set list of genes. The curated gene sets were screened against the microarray data set, and enrichment plots were generated for each gene set. An enrichment plot displays a running enrichment score as a function of the rank-ordered probes in the microarray data set. To adjust for multiple hypothesis testing, the ES for each gene was normalized to account for the size of the set, yielding a normalized enrichment score (NES). The proportion of false positives was controlled for by calculating the false discovery rate (FDR) corresponding to each NES.[27,28]

Pathway Analysis

Differentially expressed genes that met our criteria of selection were also analyzed for global functions, network, and canonical pathways (Ingenuity Pathway Analysis; Ingenuity Systems, Redwood City, CA). A spreadsheet (Excel; Microsoft, Redmond, WA) of our data containing a gene list with gene identifiers and corresponding changes was entered into the system, and patterns of differential gene expression were compared with those in the knowledge base (Pathways Knowledge Base; Ingenuity Systems).

Results

Characterization of A$\beta_{1\text{-}40}$ Oligomers

After incubation for 48 hours, A$\beta_{1\text{-}40}$ oligomers were examined with the use of AFM and immunodot blot assay. AFM analysis showed that the oligomeric preparations were composed of small globular structures with a distinct lack of fibrils (Fig. 1A). These results were consistent with those in previous studies.[29–31] Dot blot examination with the anti-oligomeric specific antibody (A11) further confirmed the presence of oligomeric structures as it reacted positively with our A$\beta_{1\text{-}40}$ samples (Fig. 1B). Furthermore, the A11 antibody did not react against a fibrillar standard sample of A$\beta_{1\text{-}40}$, confirming the specificity of the antibody to the oligomeric form.

RPE Cell Viability after Stimulation with A$\beta_{1\text{-}40}$ Oligomers

We used an MTT reduction assay to examine the effects of A$\beta_{1\text{-}40}$ and the reverse peptide A$\beta_{40\text{-}1}$ on viability of confluent RPE. Figure 2A shows the dose-dependent effects of A$\beta_{1\text{-}40}$ stimulation (0.001–0.3 μM) at 3 hours. Note that the reverse peptide A$\beta_{40\text{-}1}$ had a minor effect on the viability of RPE (97% ± 0.05% SD), compared with the DMEM control (100%). We also tested the effects of several doses of A$\beta_{1\text{-}40}$ (0.01–10.0 μM) on RPE cell viability at the 24-hour exposure time. At 0.01 μM A$\beta_{1\text{-}40}$ oligomers, the lowest dose, mean (SD) cell viability was measured to be 81% (0.08%) and decreased to 25% (0.06%) at 10.0 μM (Fig. 2B). We also examined the effects of 0.3 μM A$\beta_{1\text{-}40}$ on the viability of RPE at 3, 6, 12, and 24 hours. Note that cell survival gradually dropped from 83% (0.03%) at 3 hours to 57% (0.07%) relative to the corresponding control cultures by 24 hours (Fig. 2C).

Gene Expression Analysis of RPE Cells after A$\beta_{1\text{-}40}$ Stimulation

Analysis of the gene expression response of RPE cells after 0.3 μM A$\beta_{1\text{-}40}$ treatment was undertaken by using whole-genome oligo arrays (Agilent). At 24 hours, we observed 63 upregulated and 20 downregulated previously known genes (Tables 1, 2). The upregulated genes were found predominantly in the immune response category, but several other categories were also represented, including apoptosis, transcription factors, transporters, cell proliferation, cell signaling, and signal transduction. The three upregulated genes that exhibited the greatest changes were *IL-1β* (4.8 ± 0.49-fold), *RSAD2* (2.58± 0.57-fold), and *IL-8* (2.38 ± 0.42-fold). Relatively few genes were downregulated in response to A$\beta_{1\text{-}40}$ stimulation. Categories of downregulated genes also included immune response, transporters, cell metabolism, and transcription factors.

Confirmation of Differentially Expressed Genes after A$\beta_{1\text{-}40}$ Stimulation

Real-time qRT-PCR was performed to validate 18 genes of interest that were shown to be differentially regulated by the microarray (black bars, Fig. 3). The gene-specific primer sequences used for qRT-PCR are shown in Table 3. The amplified product for a housekeeping gene, *GAPDH*, was used as a normalizer and endogenous control. The qRT-PCR-derived validation of the direction and level of expression of the 18 selected genes is displayed in Figure 3 (white bars). The direction of expression was validated by qRT-PCR in 17 of the 18 genes. The Pearson's correlation coefficient of the PCR and microarray data for the 17 of the 18 genes was 0.65. The single gene that did not validate in the direction of expression with qRT-PCR was thrombospondin, type I, domain containing 1 (*THSD1*), which the microarray identified as downregulated (−1.64 fold) and RT-PCR identified as upregulated (+1.53-fold).

We also performed qRT-PCR for selected genes after stimulation of RPE cells with the reverse peptide (A$\beta_{40\text{-}1}$). qRT-PCR was performed for the 17 genes of interest obtained from the microarray analysis (Agilent) that were differentially upregulated after A$\beta_{1\text{-}40}$ stimulation. The amplified product for the same housekeeping gene, *GAPDH*, was used as a normalizer and endogenous control. As expected, stimulation with the control reverse peptide (A$\beta_{40\text{-}1}$) resulted in changes that were insignificant (Fig. 3, gray bars) relative to those observed after A$\beta_{1\text{-}40}$ stimulation (Fig. 3, white bars).

Supernatant Studies

Analysis of supernatants from the RPE cell culture was performed to identify the secreted levels of selected gene products. Among the three gene products (*IL-8*, *IL-1β*, *TNFSF10* [*TRAIL*]) examined, only *IL-8* was detected in significant amounts in the supernatant samples. After stimulation with A$\beta_{1\text{-}40}$ for 24 hours, the RPE cells secreted *IL-8* at an increased level compared with the untreated RPE cells. As shown in Figure 4, the amount of secreted *IL-8* was 91% higher than in the control untreated group.

Pathway Analysis

Using the mRNA expression profiles of human RPE cells treated with A$\beta_{1\text{-}40}$, we sought to determine the functional gene sets that correlated highly with our gene expression data using two types of pathway analysis. GSEA analysis identified 50 significantly enriched gene sets that correlated with the genes induced after A$\beta_{1\text{-}40}$ treatment. Many of these gene sets are highly enriched with genes related to immune response and inflammatory processes. Table 4 lists some of the top gene sets selected by the GSEA analysis. Note that all sets include genes associated with inflammatory processes. After 24 hours, the A$\beta_{1\text{-}40}$ treatment induced strong activation of genes associated with the interferon signaling pathway, immune signaling pathways, and the *NF-κB* signaling pathway involved in inflammatory processes (NES ≥ 2.03). Leading-edge analysis of gene set 13 in Table 4 within GSEA uncovered a subset of genes, including *IL-1β* and *IL-8*, within this gene set that was principally responsible for the total enrichment score (Table 5). As *IL-1β* and *-8* were both upregulated in our data set, the GSEA analysis highlights the significance of inflammatory processes in the major pathways activated after A$\beta_{1\text{-}40}$ stimulation in our study. Complementary GSEA analysis was unable to identify any pathways significantly enriched with A$\beta_{1\text{-}40}$ downregulated genes. Figure 5 lists the top genes that appear across multiple enriched gene sets from the GSEA analysis. The leading-edge analysis of our microarray data identified genes highly correlated with inflammation, immune response, interferon-regulated genes, neurodegeneration, and apoptosis.

Pathway analysis of differentially expressed genes that reached criteria in our A$\beta_{1\text{-}40}$ stimulation studies revealed the top six gene networks that reach threshold ($P < 0.05$) are leukocyte extravasation signaling, natural killer cell signaling, hepatic cholestasis, FXR/RXR activation, *IL-10* signaling, and the complement activation (Fig. 6).

Discussion

Proinflammatory Cytokines and Chemokines

Inflammation has been strongly implicated in the pathogenesis of AMD, but the initiation of the inflammatory processes in AMD is not well understood.[4,10–12] In this study, we hypothesized that A$\beta_{1\text{-}40}$, a component of drusen, is a candidate trigger of inflammatory processes in the retina. Aβ is known to activate the classic and alternative complement pathways in neuronal systems.[10,14,15,40–43] The results of our study demonstrated that treatment of human RPE cells with the oligomeric form of A$\beta_{1\text{-}40}$ (0.3 μM) for 24 hours resulted in the upregulation of a number of inflammation-associated genes, as shown by microarray and later verified by RT PCR. The top three genes with the greatest increase after

A$\beta_{1\text{-}40}$ challenge were *IL-1β*, *RSAD2*, and *IL-8*. Gene set pathway analysis also concurred that the bulk of the gene responses in our study overlap with genes associated with inflammatory processes in the public databases. These results provide further support to the hypothesis that Aβ may trigger inflammatory responses in the RPE/choroidal layers of the eye.

IL-1β is an important proinflammatory cytokine that stimulates the activation of macrophages, and the production of cytokines such as *IFN-γ*,[44–49] which promotes the upregulation of interferon α-inducible protein 27 (*IFI27*) in several types of cell lines.[50] In our studies, *IFI27* was upregulated after A$\beta_{1\text{-}40}$ treatment and suggests that activation of pathways associated with *IFN-γ* are downstream of A$\beta_{1\text{-}40}$ stimulation. Recently, Wu et al.[51] showed that *IFN-γ*, along with oxidative stress, downregulates the complement inhibitor *CFH*, which could lead to increased complement activation, a known risk factor in AMD. Our studies revealed that A$\beta_{1\text{-}40}$ stimulation of PE cells lead to *IL-1β* upregulation. In the context of the diseased eye, it is conceivable that interactions between *IL-1β* and reactive oxygen species (ROS) in the retina induce down-regulation of *CFH* and thus promote chronic inflammation. More studies are needed to further evaluate the downstream pathways associated with A$\beta_{1\text{-}40}$ stimulation.

IL-1β was also shown to induce ROS in RPE cells.[52] It is believed that ROS production may promote secretion of *IL-8* in RPE cells.[53,54] Thus, it is also possible that *IL-1β* can regulate the expression of *IL-8* in RPE by direct and indirect (via ROS) mechanisms in RPE.[52,53,55,56] Because of its chemotaxic abilities, *IL-8* release may account for the observed accumulation of inflammatory cells in the regions of drusen formation in patients with AMD. The recruitment of macrophages and neutrophils and other proinflammatory cells that produce and release proteinases and angiogenic factors into drusen could also promote neovascular events associated with the wet form of AMD.[57–59]

Although, the mRNA of both *IL-1β* and *-8* were significantly expressed, ELISA only detected *IL-8* protein in the supernatant, perhaps because the *IL-1β* precursor protein has been shown to possess a short half-life.[60]

RSAD2, or viperin, was upregulated 2.58-fold in our studies. *RSAD2* is a virus inducible antiviral protein associated with the innate immune response.[61] It is upregulated in atherosclerotic plaques and inducible in endothelial cells by stimulation with *LPS*, *IFN-γ*, or cytomegalovirus. This is the first report that RPE cells can differentially express *RSAD2*. Its specific role in AMD pathogenesis is not yet known.

CFI and *CFH*

In this study, we also observed increased gene expression of complement factor I (*CFI*), which is a known inhibitor of the complement system. *CFI* inhibits complement activation by inactivating complement component 3b (*C3b*); dysregulation of *CFI* promotes uncontrolled complement activation.[18,62,63] Recently, Fagerness et al.[64] identified a variant in the *CFI* gene that is associated with an increased risk of developing AMD. Wang et al.[18] discovered that Aβ stimulation of RPE cells resulted in the inability of *CFI* to cleave active *C3b* into its inactive form (iC3b). Although the mechanism remains unknown, Aβ is thought

to bind to *CFI* and consequently inhibits its regulatory function and causes unregulated complement activation.[18] Future studies are needed to determine the interactions between Aβ and *CFI* that cause its dysregulation of the complement pathways and the subsequent effects on RPE function. In addition to *CFI*, there is evidence in the literature supporting involvement of *CFH*, another inhibitor of the complement cascade, based its known polymorphism in AMD.[65–68] However, there was no evidence in our study or in Wang et al.[18] of A$\beta_{1\text{-}40}$-induced changes in the expression of *CFH* in human RPE cells. This finding may relate to the interactions discussed by Wu et al.[51] in which *IFN-*γ, along with oxidative stress, downregulated the complement inhibitor *CFH*.

Angiogenic Factors

A$\beta_{1\text{-}40}$-treated RPE cells were also observed to express several angiogenesis-related genes. We observed an increased gene expression of somatostatin receptor 2 (*SSTR2*) and fibronectin (*FN*) in RPE cells after treatment with Aβ. Somatostatin is a neuropeptide with antiproliferative effects in a variety of normal and cancerous cells.[69–73] Along with its receptor *SSTR2*, somatostatin has been identified in the RPE cells and has been demonstrated to inhibit *VEGF* mRNA expression,[74] a finding that is consistent with our results. On the other hand, Yoshida et al.[17] showed that stimulation of human RPE cells with A$\beta_{1\text{-}40}$ resulted in the altered expression of angiogenic genes, specifically vascular endothelial growth factor (*VEGF*). Although we did not observe changes in the levels of *VEGF* expression in our study, possibly due to the inhibitory effects of somatostatin on *VEGF* mRNA expression, the differences may also be due to the specific time courses and doses of A$\beta_{1\text{-}40}$ used in each study.

Another upregulated gene, *FN*, which codes for an extracellular matrix (ECM) glycoprotein, may also play a role in angiogenesis. It is possible that altered levels of ECM genes, including *FN*, can lead to abnormal RPE-choriocapillaris behavior.[8]

Apoptotic Mechanisms

The effect of the oligomeric form of A$\beta_{1\text{-}40}$ on RPE cell viability was assessed by MTT. Several apoptotic genes were upregulated in the microarray study and support the reduction in cell viability observed in the MTT study. qRT-PCR studies showed increased gene expression of two important caspase-independent apoptotic genes, tumor necrosis factor related apoptosis-inducing ligand (*TNFSF10* or *TRAIL*) and X-linked inhibitor of apoptosis associated factor 1 (*XAF1*). *TRAIL*, a member of the *TNF* superfamily, is expressed in several cell types and is activated by Aβ stimulation in neurons. It is believed that *TRAIL* expression promotes apoptotic cell death, as neutralization of *TRAIL* protects against Aβ toxicity in a human neuronal cell line.[75]

XAF1, another gene upregulated in our stimulation studies, interacts with *XIAP* to block its anticaspase activity.[75] In earlier studies *XAF1* was identified in several screens as a key mediator of apoptosis and was recently shown to dramatically sensitize cancer cells to apoptotic triggers such as *TN-FSF10*.[76,77] Accordingly, it has been shown that interferon-induced apoptosis is mediated by the overexpression of *XAF1*, which is believed to increase susceptibility to *TRAIL*-induced cytotoxicity.[77] Thus, in our studies, A$\beta_{1\text{-}40}$ stimulation of

RPE cells may have activated cell death in the RPE via *XAF1* and *TNFSF10* activity, as both genes were significantly upregulated in our study and have been shown to increase apoptosis in cancer cells.[78]

Our results also showed an increased expression of *CYP2D6*, a member of the cytochrome P450 family that is involved in the first line of defense against oxidative stress and has been shown to detoxify reactive oxygen species (ROS).[79] A$\beta_{1\text{-}40}$ stimulation of RPE cells in our study may also initiate ROS-induced signaling pathways, including stress-activated protein kinases and nuclear transcription factor *NF-κB*.[52,80–82] *NF-κB* is upregulated by *IL-8* and has been implicated in retinal neovascularization.[47,83]

Proposed Interaction of Gene Products Differentially Expressed in RPE after A$\beta_{1\text{-}40}$ Stimulation

In conclusion, our in vitro studies lend support to the hypothesis that A$\beta_{1\text{-}40}$ promotes local inflammation near drusen sites and within the surrounding RPE layer that may promote the pathogenesis of AMD.[3,10,17] Our finding that RPE cells upregulate several genes associated with proinflammatory cytokines (*IL-1β*, *IL-8*), interferon-inducible proteins (*IFI27*, *IFI44L*), an inhibitor of the complement cascade (*CFI*), and an inhibitor of oxidative stress (*CYP2D6*) in response to A$\beta_{1\text{-}40}$ challenge, may present a novel mechanism and partial explanation for the onset of inflammation in the eye near drusen sites. A summary schematic that illustrates the proposed circuitry by which A$\beta_{1\text{-}40}$ may affect RPE gene expression leading to inflammatory events in the eye is shown in Figure 7. We hypothesize that A$\beta_{1\text{-}40}$, known already to be present in drusen of AMD eyes, may induce RPE cells to secrete proinflammatory cytokines in which *IL-1β* may subsequently further promote overexpression of *IL-8* via several known mechanisms, including ROS production.[53,54] *IL-8*, an important chemokine, may promote migration and activation of immune cells (neutrophils, macrophages) toward the RPE.[82,85,86] The accumulation of neutrophils, macrophages, and microglial cells may cause further pathologic changes in the RPE and Bruch's membrane complex.[4,8,9,81,87] Our results also suggest that, A$\beta_{1\text{-}40}$ may promote RPE cells to overexpress *CFI*. Other in vitro studies showed that the interactions between A$\beta_{1\text{-}40}$ and *CFI* cause *CFI* to lose its complement regulatory function.[18,62] In the absence of *CFI*, unregulated complement activation would take place resulting in increased inflammation.[18] Furthermore, A$\beta_{1\text{-}40}$ may also cause RPE cells to secrete *IFN-γ*. According to Wu et al.[51] *IFN-γ* (along with oxidative stress) may reduce *CFH* activity, thus increasing complement activation that may further promote AMD disease progression.

Acknowledgments

Supported by Canadian Institute of Health Research (CIHR) Grant MOP-97806 (JM) and MOP-77736.

The authors thank Li Yu for RT-PCR analysis, Eleanor To for assistance with the illustrations, and Fanny Chu for assistance with AFM measurements.

References

1. Abdelsalam A, Del Priore L, Zarbin MA. Drusen in age-related macular degeneration: pathogenesis, natural course, and laser photocoagulation-induced regression. Surv Ophthalmol. 1999; 44:1–29. [PubMed: 10466585]

2. Johnson PT, Lewis GP, Talaga KC, et al. Drusen-associated degeneration in the retina. Invest Ophthalmol Vis Sci. 2003; 44:4481–4488. [PubMed: 14507896]
3. Luibl V, Isas JM, Kayed R, Glabe CG, Langen R, Chen J. Drusen deposits associated with aging and age-related macular degeneration contain nonfibrillar amyloid oligomers. J Clin Invest. 2006; 116:378–385. [PubMed: 16453022]
4. Anderson DH, Mullins RF, Hageman GS, Johnson LV. A role for local inflammation in the formation of drusen in the aging eye. Am J Ophthalmol. 2002; 134:411–431. [PubMed: 12208254]
5. Seth A, Cui J, To E, Kwee M, Matsubara J. Complement-associated deposits in the human retina. Invest Ophthalmol Vis Sci. 2008; 49:743–750. [PubMed: 18235023]
6. Johnson LV, Leitner WP, Staples MK, Anderson DH. Complement activation and inflammatory processes in drusen formation and age related macular degeneration. Exp Eye Res. 2001; 73:887–896. [PubMed: 11846519]
7. Hageman GS, Luthert PJ, Victor Chong NH, Johnson LV, Anderson DH, Mullins RF. An integrated hypothesis that considers drusen as biomarkers of immune-mediated processes at the RPE-Bruch's membrane interface in aging and age-related macular degeneration. Prog Retin Eye Res. 2001; 20:705–732. [PubMed: 11587915]
8. Zarbin MA. Current concepts in the pathogenesis of age-related macular degeneration. Arch Ophthalmol. 2004; 122:598–614. [PubMed: 15078679]
9. Bok D. Evidence for an inflammatory process in age-related macular degeneration gains support. Proc Natl Acad Sci. 2005; 102(20):7053–7054. [PubMed: 15886281]
10. Johnson LV, Leitner WP, Rivest AJ, Staples MK, Radeke MJ, Anderson DH. The Alzheimer's A β-peptide is deposited at sites of complement activation in pathologic deposits associated with aging and age-related macular degeneration. Proc Natl Acad Sci USA. 2002; 99:11830–11835. [PubMed: 12189211]
11. McGeer PL, McGeer EG. Inflammation and the degenerative diseases of aging. Ann NY Acad Sci. 2004; 1035:104–116. [PubMed: 15681803]
12. Donoso LA, Kim D, Frost A, Callahan A, Hageman G. The role of inflammation in the pathogenesis of age-related macular degeneration. Surv Ophthalmol. 2006; 51:137–152. [PubMed: 16500214]
13. Mullins RF, Russell SR, Anderson DH, Hageman GS. Drusen associated with aging and age-related macular degeneration contain proteins common to extracellular deposits associated with atherosclerosis, elastosis, amyloidosis, and dense deposit disease. FASEB J. 2000; 14:835–846. [PubMed: 10783137]
14. Anderson DH, Talaga KC, Rivest AJ, Barron E, Hageman GS, Johnson LV. Characterization of beta amyloid assemblies in drusen: the deposits associated with aging and age-related macular degeneration. Exp Eye Res. 2004; 78:243–256. [PubMed: 14729357]
15. Dentchev T, Milam AH, Lee VM, Trojanowski JQ, Dunaief JL. Amyloid-beta is found in drusen from some age-related macular degeneration retinas, but not in drusen from normal retinas. Mol Vis. 2003; 9:184–190. [PubMed: 12764254]
16. Ning A, Cui J, To E, et al. Amyloid-beta deposits lead to retinal degeneration in a mouse model of Alzheimer disease. Invest Ophthalmol Vis Sci. 2008; 49(11):5136–5143. [PubMed: 18566467]
17. Yoshida T, Ohno-Matsui K, Ichinose S, et al. The potential role of amyloid beta in the pathogenesis of age-related macular degeneration. J Clin Invest. 2005; 115:2793–2800. [PubMed: 16167083]
18. Wang J, Ohno-Matsui K, Yoshida T, et al. Altered function of factor I caused by amyloid beta: implication for pathogenesis of age-related macular degeneration from drusen. J Immunol. 2008; 181:712–720. [PubMed: 18566438]
19. Bruban J, Glotin AL, Dinet V, et al. Amyloid-β(1-42) alters structure and function of retinal pigmented epithelial cells. Aging Cell. 2009; 8:162–177. [PubMed: 19239420]
20. Kayed R, Head E, Thompson JL, et al. Common structure of soluble amyloid oligomers implies common mechanism of pathogenesis. Science. 2003; 300:486–489. [PubMed: 12702875]
21. Stine WB Jr, Snyder SW, Ladror US, et al. The nanometer-scale structure of amyloid-beta visualized by atomic force microscopy. J Protein Chem. 1996; 15:193–203. [PubMed: 8924204]
22. Chromy BA, Nowak RJ, Lambert MP, et al. Self-assembly of abeta(1-42) into globular neurotoxins. Biochemistry. 2003; 42:12749–12760. [PubMed: 14596589]

23. Wang XF, Cui JZ, Prasad SS, Matsubara JA. Altered gene expression of angiogenic factors induced by calcium-mediated dissociation of retinal pigment epithelial cells. Invest Ophthalmol Vis Sci. 2005; 46:1508–1515. [PubMed: 15790923]
24. Gamulescu MA, Chen Y, He S, et al. Transforming growth factor beta2-induced myofibroblastic differentiation of human retinal pigment epithelial cells: Regulation by extracellular matrix proteins and hepatocyte growth factor. Exp Eye Res. 2006; 83:212–222. [PubMed: 16563380]
25. Wang XF, Cui JZ, Nie W, Prasad SS, Matsubara JA. Differential gene expression of early and late passage retinal pigment epithelial cells. Exp Eye Res. 2004; 79:209–221. [PubMed: 15325568]
26. Talaat AM, Howard ST, Hale W 4th, Lyons R, Garner H, Johnston SA. Genomic DNA standards for gene expression profiling in mycobacterium tuberculosis. Nucleic Acids Res. 2002; 30:e104. [PubMed: 12384606]
27. Mootha VK, Lindgren CM, Eriksson KF, et al. PGC-1alpha-responsive genes involved in oxidative phosphorylation are coordinately downregulated in human diabetes. Nat Genet. 2003; 34:267–273. [PubMed: 12808457]
28. Subramanian A, Tamayo P, Mootha VK, et al. Gene set enrichment analysis: a knowledge-based approach for interpreting genome-wide expression profiles. Proc Natl Acad Sci USA. 2005; 102:15545–15550. [PubMed: 16199517]
29. Lambert MP, Barlow AK, Chromy BA, et al. Diffusible, nonfibrillar ligands derived from Abeta1-42 are potent central nervous system neurotoxins. Proc Natl Acad Sci USA. 1998; 95:6448–6453. [PubMed: 9600986]
30. Lambert MP, Viola KL, Chromy BA, et al. Vaccination with soluble abeta oligomers generates toxicity-neutralizing antibodies. J Neurochem. 2001; 79:595–605. [PubMed: 11701763]
31. Dahlgren KN, Manelli AM, Stine WB Jr, Baker LK, Krafft GA, LaDu MJ. Oligomeric and fibrillar species of amyloid-beta peptides differentially affect neuronal viability. J Biol Chem. 2002; 277:32046–32053. [PubMed: 12058030]
32. Leong WF, Tan HC, Ooi EE, Koh DR, Chow VT. Microarray and real-time RT-PCR analyses of differential human gene expression patterns induced by severe acute respiratory syndrome (SARS) coronavirus infection of vero cells. Microbes Infect. 2005; 7:248–259. [PubMed: 15777647]
33. Kroismayr R, Baranyi U, Stehlik C, Dorfleutner A, Binder BR, Lipp J. HERC5, a HECT E3 ubiquitin ligase tightly regulated in LPS activated endothelial cells. J Cell Sci. 2004; 117:4749–4756. [PubMed: 15331633]
34. Overbeck S, Uciechowski P, Ackland ML, Ford D, Rink L. Intracellular zinc homeostasis in leukocyte subsets is regulated by different expression of zinc exporters ZnT-1 to ZnT-9. J Leukoc Biol. 2008; 83:368–380. [PubMed: 17971500]
35. Carriere V, Roussel L, Ortega N, et al. IL-33, the IL-1-like cytokine ligand for ST2 receptor, is a chromatin-associated nuclear factor in vivo. Proc Natl Acad Sci USA. 2007; 104:282–287. [PubMed: 17185418]
36. Komatsuda A, Wakui H, Iwamoto K, et al. Upregulation of TRAIL mRNA expression in peripheral blood mononuclear cells from patients with active systemic lupus erythematosus. Clin Immunol. 2007; 125:26–29. [PubMed: 17683987]
37. Kempkensteffen C, Hinz S, Schrader M, et al. Gene expression and promoter methylation of the XIAP-associated factor 1 in renal cell carcinomas: Correlations with pathology and outcome. Cancer Lett. 2007; 254:227–235. [PubMed: 17449173]
38. Kojima K, Nagata K, Matsubara T, Yamazoe Y. Broad but distinct role of pregnane x receptor on the expression of individual cytochrome p450s in human hepatocytes. Drug Metab Pharmacokinet. 2007; 22:276–286. [PubMed: 17827782]
39. Kumar M, Liu ZR, Thapa L, Qin RY. Anti-angiogenic effects of somatostatin receptor subtype 2 on human pancreatic cancer xenografts. Carcinogenesis. 2004; 25:2075–2081. [PubMed: 15205362]
40. McGeer PL, Akiyama H, Itagaki S, McGeer EG. Activation of the classical complement pathway in brain tissue of Alzheimer patients. Neurosci Lett. 1989; 107:341–346. [PubMed: 2559373]
41. Webster S, Lue LF, Brachova L, et al. Molecular and cellular characterization of the membrane attack complex, C5b-9, in Alzheimer's disease. Neurobiol Aging. 1997; 18:415–421. [PubMed: 9330973]

42. Shen Y, Li R, McGeer EG, McGeer PL. Neuronal expression of mRNAs for complement proteins of the classical pathway in Alzheimer brain. Brain Res. 1997; 769:391–395. [PubMed: 9374212]
43. Akiyama H, Barger S, Barnum S, et al. Inflammation and Alzheimer's disease. Neurobiol Aging. 2000; 21:383–421. [PubMed: 10858586]
44. Planck SR, Huang XN, Robertson JE, Rosenbaum JT. Retinal pigment epithelial cells produce interleukin-1 beta and granulocyte-macrophage colony-stimulating factor in response to interleukin-1 alpha. Curr Eye Res. 1993; 12:205–212. [PubMed: 8482109]
45. Jaffe GJ, Roberts WL, Wong HL, Yurochko AD, Cianciolo GJ. Monocyte-induced cytokine expression in cultured human retinal pigment epithelial cells. Exp Eye Res. 1995; 60:533–543. [PubMed: 7615019]
46. Elner VM, Elner SG, Standiford TJ, Lukacs NW, Strieter RM, Kunkel SL. Interleukin-7 (IL-7) induces retinal pigment epithelial cell MCP-1 and *IL-8*. Exp Eye Res. 1996; 63:297–303. [PubMed: 8943702]
47. Yoshida A, Yoshida S, Khalil AK, Ishibashi T, Inomata H. Role of NF-kappaB-mediated interleukin-8 expression in intraocular neovascularization. Invest Ophthalmol Vis Sci. 1998; 39:1097–1106. [PubMed: 9620068]
48. Holtkamp GM, Van Rossem M, de Vos AF, Willekens B, Peek R, Kijlstra A. Polarized secretion of IL-6 and *IL-8* by human retinal pigment epithelial cells. Clin Exp Immunol. 1998; 112:34–43. [PubMed: 9566787]
49. Poleganov MA, Pfeilschifter J, Muhl H. Expanding extracellular zinc beyond levels reflecting the albumin-bound plasma zinc pool potentiates the capability of IL-1beta, IL-18, and IL-12 to act as *IFN*-gamma-inducing factors on PBMC. J Interferon Cytokine Res. 2007; 27:997–1001. [PubMed: 18184040]
50. Gjermandsen IM, Justesen J, Martensen PM. The interferon-induced gene ISG12 is regulated by various cytokines as the gene 6–16 in human cell lines. Cytokine. 2000; 12:233–238. [PubMed: 10704250]
51. Wu Z, Lauer TW, Sick A, Hackett SF, Campochiaro PA. Oxidative stress modulates complement factor H expression in retinal pigmented epithelial cells by acetylation of FOXO3. J Biol Chem. 2007; 282:22414–22425. [PubMed: 17558024]
52. Yang D, Elner SG, Bian ZM, Till GO, Petty HR, Elner VM. Pro-inflammatory cytokines increase reactive oxygen species through mitochondria and NADPH oxidase in cultured RPE cells. Exp Eye Res. 2007; 85:462–472. [PubMed: 17765224]
53. Elner VM, Strieter RM, Elner SG, Baggiolini M, Lindley I, Kunkel SL. Neutrophil chemotactic factor (*IL-8*) gene expression by cytokine-treated retinal pigment epithelial cells. Am J Pathol. 1990; 136:745–750. [PubMed: 2183623]
54. Bian ZM, Elner SG, Yoshida A, Elner VM. Differential involvement of phosphoinositide 3-kinase/Akt in human RPE MCP-1 and *IL-8* expression. Invest Ophthalmol Vis Sci. 2004; 45:1887–1896. [PubMed: 15161854]
55. Baggiolini M, Dewald B, Moser B. Interleukin-8 and related chemotactic cytokines: CXC and CC chemokines. Adv Immunol. 1994; 55:97–179. [PubMed: 8304236]
56. Hwang YS, Jeong M, Park JS, et al. Interleukin-1beta stimulates *IL-8* expression through MAP kinase and ROS signaling in human gastric carcinoma cells. Oncogene. 2004; 23:6603–6611. [PubMed: 15208668]
57. Higgins GT, Wang JH, Dockery P, Cleary PE, Redmond HP. Induction of angiogenic cytokine expression in cultured RPE by ingestion of oxidized photoreceptor outer segments. Invest Ophthalmol Vis Sci. 2003; 44:1775–1782. [PubMed: 12657621]
58. Killingsworth MC, Sarks JP, Sarks SH. Macrophages related to Bruch's membrane in age-related macular degeneration. Eye. 1990; 4(Pt 4):613–621. [PubMed: 2226993]
59. Heymans S, Luttun A, Nuyens D, et al. Inhibition of plasminogen activators or matrix metalloproteinases prevents cardiac rupture but impairs therapeutic angiogenesis and causes cardiac failure. Nat Med. 1999; 5:1135–1142. [PubMed: 10502816]
60. Moors MA, Mizel SB. Proteasome-mediated regulation of interleukin-1beta turnover and export in human monocytes. J Leukoc Biol. 2000; 68:131–136. [PubMed: 10914500]

61. Olofsson PS, Jatta K, Wagsater D, et al. The antiviral cytomegalovirus inducible gene 5/Viperin is expressed in atherosclerosis and regulated by proinflammatory agents. Arterioscler Thromb Vasc Biol. 2005; 25(7):e113–6. [PubMed: 15890971]
62. Sahu A, Isaacs SN, Soulika AM, Lambris JD. Interaction of vaccinia virus complement control protein with human complement proteins: factor I-mediated degradation of C3b to iC3b1 inactivates the alternative complement pathway. J Immunol. 1998; 160:5596–5604. [PubMed: 9605165]
63. Tsiftsoglou SA, Willis AC, Li P, et al. The catalytically active serine protease domain of human complement factor I. Biochemistry. 2005; 44:6239–6249. [PubMed: 15835912]
64. Fagerness JA, Maller JB, Neale BM, Reynolds RC, Daly MJ, Seddon JM. Variation near complement factor I is associated with risk of advanced AMD. Eur J Hum Genet. 2008
65. Klein RJ, Zeiss C, Chew EY, et al. Complement factor H polymorphism in age-related macular degeneration. Science. 2005; 308:385–389. [PubMed: 15761122]
66. Edwards AO, Ritter R 3rd, Abel KJ, Manning A, Panhuysen C, Farrer LA. Complement factor H polymorphism and age-related macular degeneration. Science. 2005; 308:421–424. [PubMed: 15761121]
67. Haines JL, Hauser MA, Schmidt S, et al. Complement factor H variant increases the risk of age-related macular degeneration. Science. 2005; 308:419–421. [PubMed: 15761120]
68. Chen M, Forrester JV, Xu H. Synthesis of complement factor H by retinal pigment epithelial cells is down-regulated by oxidized photoreceptor outer segments. Exp Eye Res. 2007; 84:635–645. [PubMed: 17292886]
69. Patel YC. Somatostatin and its receptor family. Front Neuroendocrinol. 1999; 20:157–198. [PubMed: 10433861]
70. Virgolini I, Yang Q, Li S, et al. Cross-competition between vasoactive intestinal peptide and somatostatin for binding to tumor cell membrane receptors. Cancer Res. 1994; 54:690–700. [PubMed: 7905785]
71. Luo Q, Peyman GA, Conway MD, Woltering EA. Effect of a somatostatin analog (octreotide acetate) on the growth of retinal pigment epithelial cells in culture. Curr Eye Res. 1996; 15:909–913. [PubMed: 8921210]
72. Albers AR, O'Dorisio MS, Balster DA, et al. Somatostatin receptor gene expression in neuroblastoma. Regul Pept. 2000; 88:61–73. [PubMed: 10706954]
73. Sall JW, Klisovic DD, O'Dorisio MS, Katz SE. Somatostatin inhibits IGF-1 mediated induction of VEGF in human retinal pigment epithelial cells. Exp Eye Res. 2004; 79:465–476. [PubMed: 15381031]
74. Lambooij AC, Kuijpers RW, van Lichtenauer-Kaligis EG, et al. Somatostatin receptor 2A expression in choroidal neovascularization secondary to age-related macular degeneration. Invest Ophthalmol Vis Sci. 2000; 41:2329–2335. [PubMed: 10892880]
75. Cantarella G, Uberti D, Carsana T, Lombardo G, Bernardini R, Memo M. Neutralization of TRAIL death pathway protects human neuronal cell line from beta-amyloid toxicity. Cell Death Differ. 2003; 10:134–141. [PubMed: 12655302]
76. Liston P, Fong WG, Kelly NL, et al. Identification of XAFI as an antagonist of XIAP anti-Caspase activity. Nat Cell Biol. 2001; 3:128–133. [PubMed: 11175744]
77. Leaman DW, Chawla-Sarkar M, Vyas K, et al. Identification of X-linked inhibitor of apoptosis-associated factor-1 as an interferon-stimulated gene that augments TRAIL Apo2L-induced apoptosis. J Biol Chem. 2002; 277:28504–28511. [PubMed: 12029096]
78. Micali OC, Cheung HH, Plenchette S, et al. Silencing of the XAFI gene by promoter hypermethylation in cancer cells and reactivation to TRAIL-sensitization by *IFN-β*. BMC Cancer. 2007; 7:52. [PubMed: 17376236]
79. Esfandiary H, Chakravarthy U, Patterson C, Young I, Hughes AE. Association study of detoxification genes in age related macular degeneration. Br J Ophthalmol. 2005; 89:470–474. [PubMed: 15774926]
80. Flohe L, Brigelius-Flohe R, Saliou C, Traber MG, Packer L. Redox regulation of NF-kappa B activation. Free Radic Biol Med. 1997; 22:1115–1126. [PubMed: 9034250]

81. Tezel TH, Bora NS, Kaplan HJ. Pathogenesis of age-related macular degeneration. Trends Mol Med. 2004; 10:417–420. [PubMed: 15350892]
82. Fernandes AF, Zhou J, Zhang X, et al. Oxidative inactivation of the proteasome in RPE: a potential link between oxidative stress and upregulation of *IL-8*. J Biol Chem. 2008 Jul 25; 283(30):20745–20753. [PubMed: 18502748]
83. Elner SG, Elner VM, Jaffe GJ, Stuart A, Kunkel SL, Strieter RM. Cytokines in proliferative diabetic retinopathy and proliferative vitreoretinopathy. Curr Eye Res. 1995; 14:1045–1053. [PubMed: 8585935]
84. Jaffe GJ, Van Le L, Valea F, et al. Expression of interleukin-1 alpha, interleukin-1 beta, and an interleukin-1 receptor antagonist in human retinal pigment epithelial cells. Exp Eye Res. 1992; 55:325–335. [PubMed: 1426065]
85. Cohen J. The immunopathogenesis of sepsis. Nature. 2002; 420:885–891. [PubMed: 12490963]
86. Tsai YY, Lin JM, Wan L, et al. Interleukin gene polymorphisms in age-related macular degeneration. Invest Ophthalmol Vis Sci. 2008; 49:693–698. [PubMed: 18235016]
87. Nowak JZ. Age-related macular degeneration (AMD): pathogenesis and therapy. Pharmacol Rep. 2006; 58:353–363. [PubMed: 16845209]

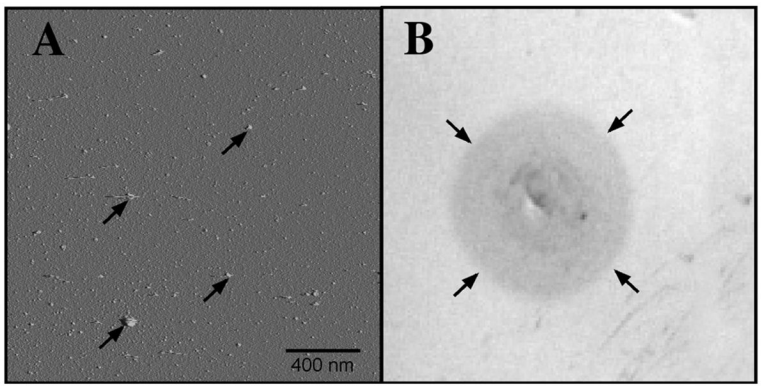

Figure 1.

Confirmation of oligomeric form of A$\beta_{1\text{-}40}$. (**A**) AFM examination of A$\beta_{1\text{-}40}$ oligomeric solution at 48 hours. The A$\beta_{1\text{-}40}$ solution was applied to freshly cleaved mica and imaged according to Chromy et al.[48] AFM image shows predominately small globular structures (*arrows*) and a distinct lack of fibrils. (**B**) Dot blot with the use of the A11 antibody shows positive staining with the A$\beta_{1\text{-}40}$ sample (*arrows*) compared to no staining in both negative control and fibrillar form of Aβ samples (Invitrogen). Primary and secondary antibodies were diluted according to manufacturer's recommendations, 1:1000 and 1:2000, respectively.

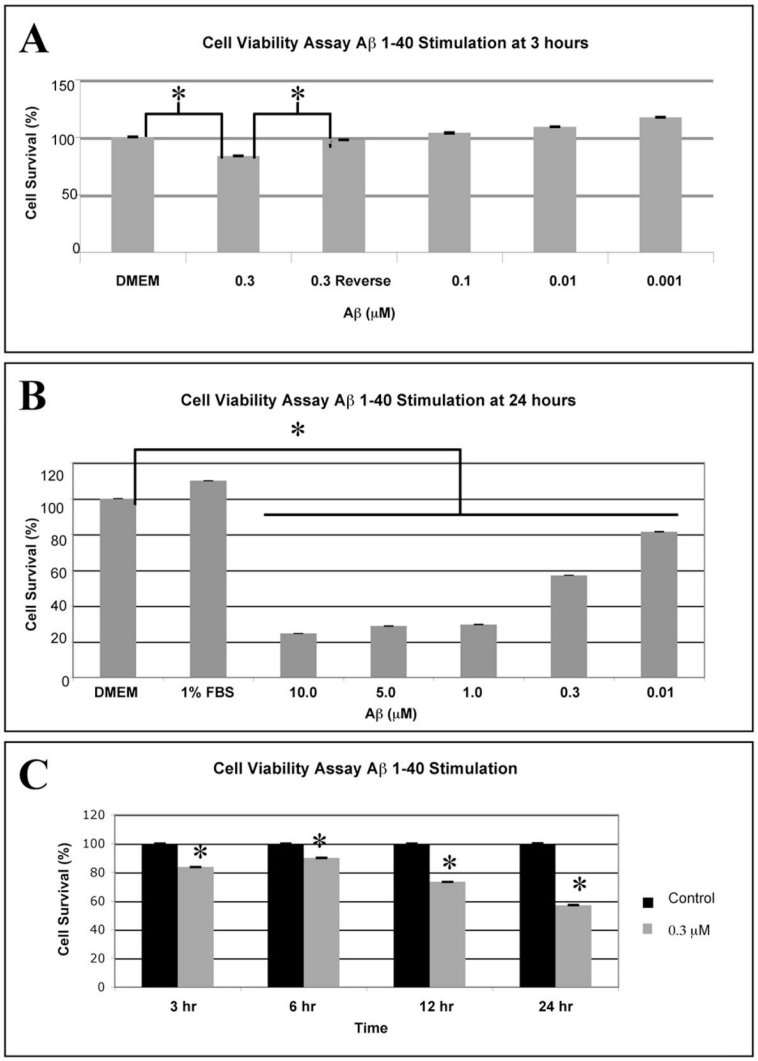

Figure 2.

MTT reduction assay for cell viability after stimulation with A$\beta_{1\text{-}40}$ or the control reverse peptide A$\beta_{40\text{-}1}$. (**A**) Confluent RPE cells were subjected to stimulation with 0.001 to 0.3 μM oligomeric A$\beta_{1\text{-}40}$ or the reverse peptide, 0.3 μM A$\beta_{40\text{-}1}$, for 3 hours. Cell viability was significantly reduced at 0.3 μM A$\beta_{1\text{-}40}$ compared with cells incubated in serum-free DMEM or to cells incubated in the control reverse peptide A$\beta_{40\text{-}1}$. Note that lower doses (0.001 to 0.1 μM A $\beta_{1\text{-}40}$) induced proliferation of the RPE. (**B**) A dose–response curve for RPE cells stimulated with 0.01- to 10.0-μM solutions of oligomeric A$\beta_{1\text{-}40}$ for 24 hours demonstrates 81% and 57% cell viability at 0.01 and 0.3 μM. Cell viability drops to <30% at concentrations of A$\beta_{1\text{-}40}$ greater than 0.3 μM. All doses resulted in significant differences with cells grown in serum free DMEM only. (**C**) Confluent RPE cells were stimulated with 0.3 μM solutions of oligomeric A$\beta_{1\text{-}40}$ at 3, 6, 12, and 24 hours. The graph depicts the mean and SD from three independent experiments. RPE cells stimulated with A$\beta_{1\text{-}40}$ at 0.3 μM displayed a time-dependent decrease in viability dropping to 58% cell viability at 24 hours as assessed with the MTT assay. A two-sample *t*-test was performed to compare the viability

of the cells in the control group (cells incubated in serum-free DMEM and not stimulated with $A\beta_{1-40}$) to that of the cells incubated in serum-free DMEM and stimulated with 0.3 μM $A\beta_{1-40}$ at each time point. Note that at all time points, the viability of the stimulation group was lower than the control (unstimulated) group ($^*P < 0.05$). The data are shown as the mean and SD of results in three independent experiments.

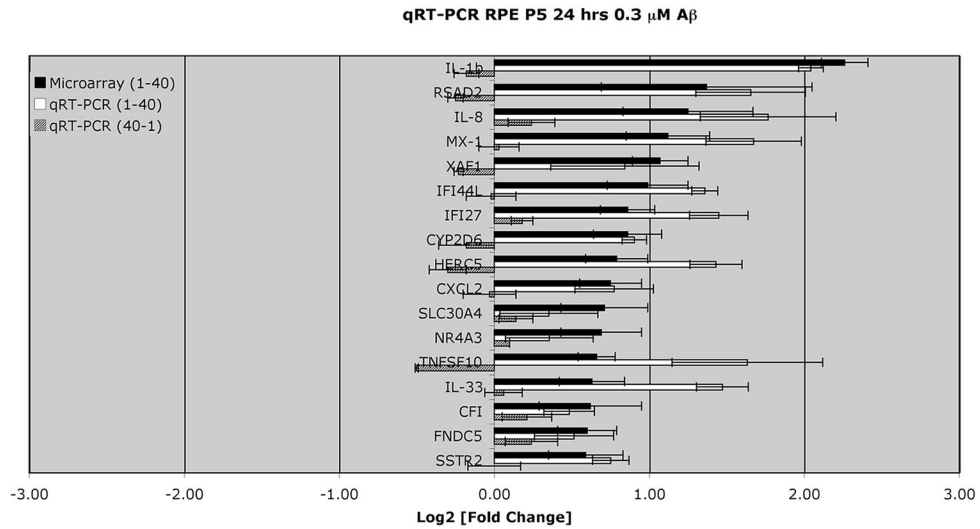

Figure 3.

Genes of interest from the differential gene expression of RPE cells stimulated by 0.3 μM A$\beta_{1\text{-}40}$ for 24 hours and analyzed by Agilent Oligo microarray were further verified by qRT-PCR. Primers used for each gene product are shown in Table 3. Note that the microarray data shown here and in Tables 1 and 2 all demonstrated a ≥1.5-fold change, and reached significance ($P < 0.05$). The largest changes were seen for cytokines, *IL-1β* and *IL-8*, and *RSAD2* (viperin). Values are expressed as relative changes ($\log_2$-fold) with respect to the corresponding controls. Data represent the mean ± SEM of three independent experiments for both microarray ($P < 0.05$) and for qRT-PCR. The Pearson's correlation coefficient of the microarray data and PCR $\log_2$ values for the 17 genes shown in the *black* and *white* bars is 0.65. These same 17 genes were also assessed after stimulation with the control reverse peptide (0.3 μM A$\beta_{40\text{-}1}$) for 24 hours by qRT PCR. Note that the changes associated with the reverse peptide were significantly lower than results obtained after 0.3 μM A$\beta_{1\text{-}40}$ stimulation.

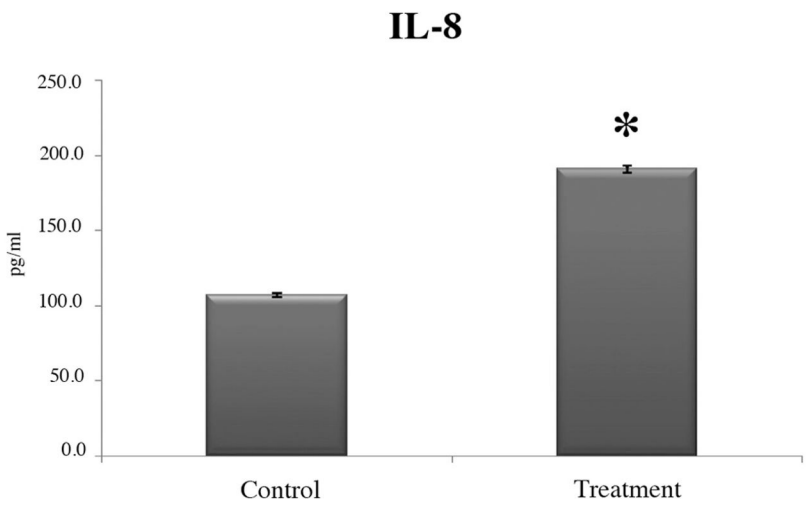

Figure 4.

Cytokine levels in cell culture supernatant samples. Human fetal RPE cells challenged with 0.3 μM $Ab_{1\text{-}40}$ oligomers for 24 hours showed increased secretion of *IL-8* by ELISA. Compared to control cells, *IL-8* secretion was increased, by approximately a factor of 2, in cultures of $Ab_{1\text{-}40}$-treated cells (*significance by *t*-test, $P < 0.05$). Mean values from three independent experiments and the SEM are shown.

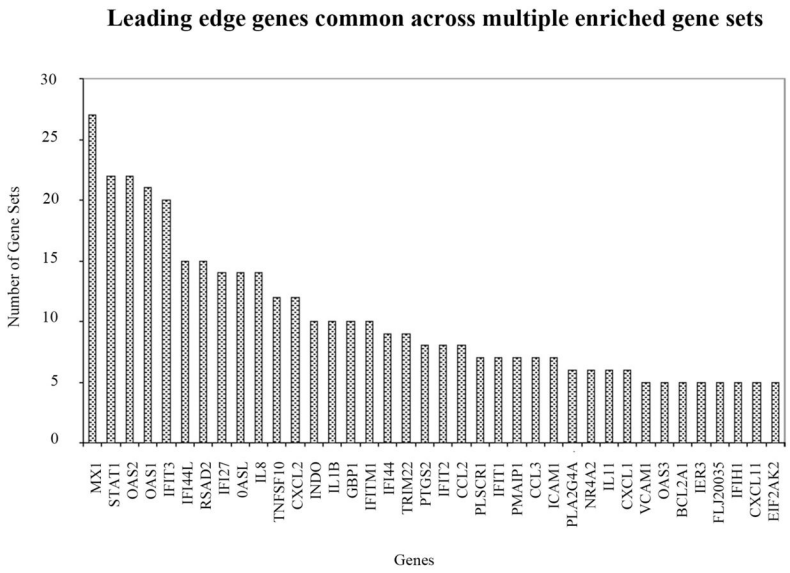

Figure 5.

GSEA leading edge gene sets analysis. The analysis selects the genes that appear across multiple enriched gene sets from the public databases. These genes are expected to have higher biological significance. The leading edge analysis of our microarray data identified gene highly correlated with inflammation, immune response, interferon-regulated genes, apoptosis, and neurodegeneration.

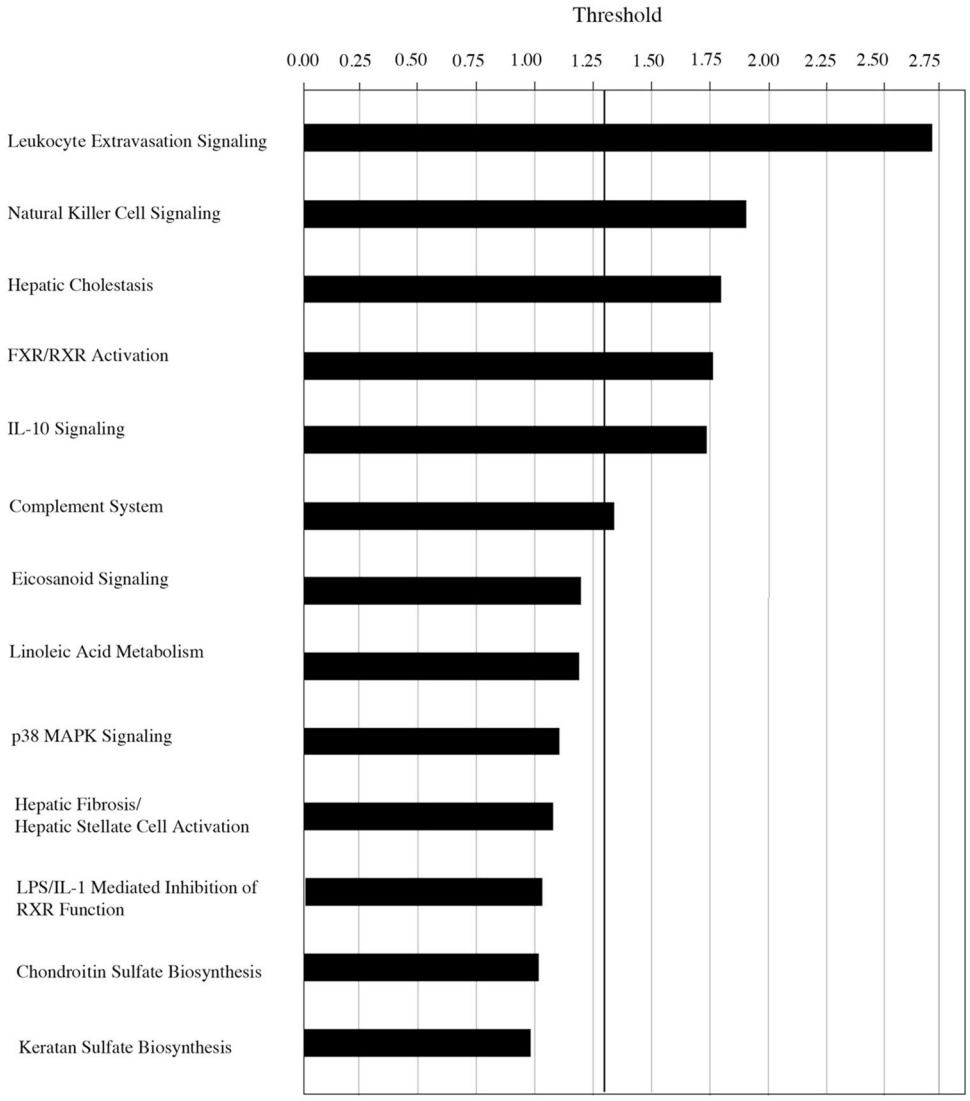

Figure 6.

Pathway analysis by Ingenuity Pathway Analysis (IPA) software program. Note that the six top-ranked pathways, leukocyte extravasation signaling, natural killer cell signaling, hepatic cholestasis, *FXR-RXR* activation, *IL-10* signaling and the complement system, reached the criteria set at $P < 0.05$. All six are associated with inflammation.

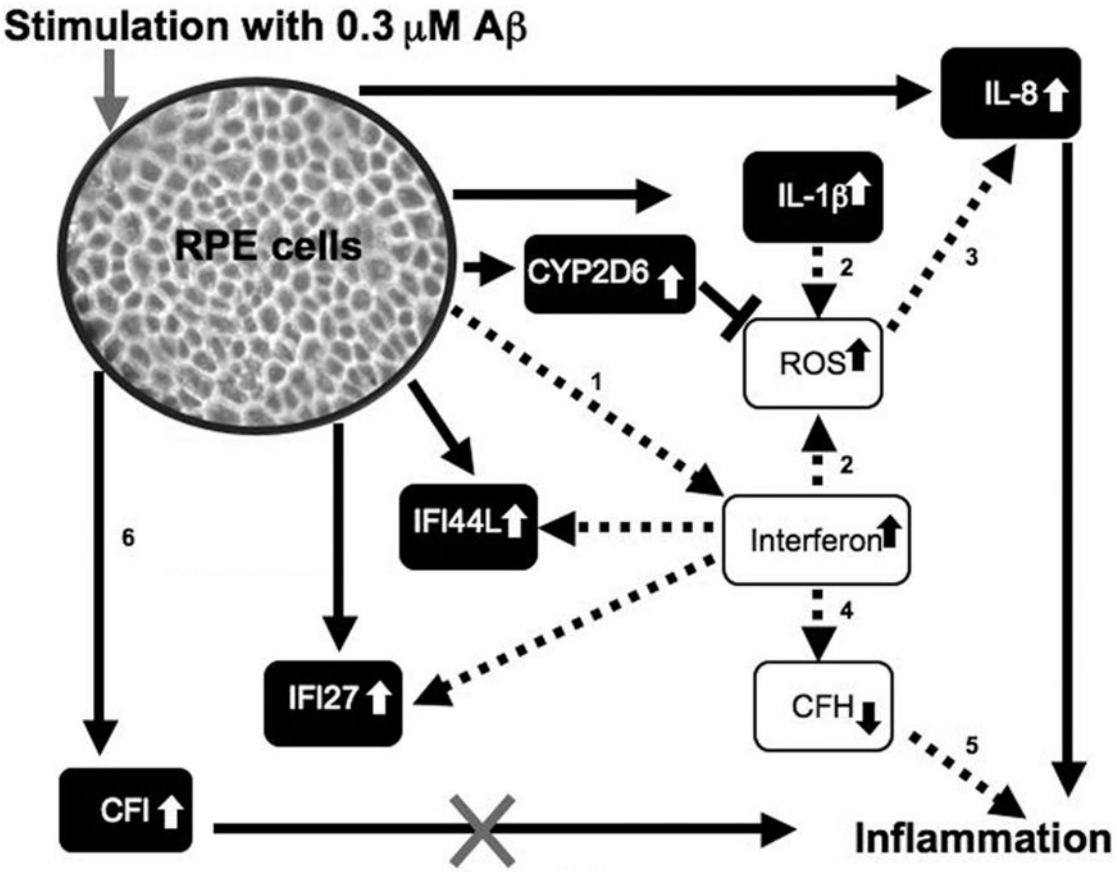

Figure 7.

Summary schematic of results obtained from A$\beta_{1\text{-}40}$ stimulation of RPE cells. After 24 hours, genes for *IL-1β*, *IL-8*, *CFI*, *CYP2DK*, *IFI44L* and *IFI27* were upregulated in response to *A*$\beta_{1\text{-}40}$ stimulation (represented by *black boxes*, *white text* and *solid lines*). *IL-1β* is known to also promote generation of ROS, which may further promote *IL-8* expression (*dashed line*). In the context of the eye, *IL-8* overexpression by RPE may promote macrophage and microglial migration toward RPE and in drusen containing Aβ. A prolonged macrophage and microglial response in the RPE/choroid layers may further support oxidative injury and inflammatory events through respiratory burst mechanisms. Genes for interferon-induced proteins (*IFI44L* and *IFI27*) were also upregulated in response to *A*$\beta_{1\text{-}40}$ stimulation in our studies. Interferon-γ, in the setting of oxidative stress, was shown to reduce *CFH* activity, and thus promote inflammation (*dashed line*). In our study, two of the genes upregulated in response to A$\beta_{1\text{-}40}$ stimulation, *CFI* and *CYP2D6*, have protective value. The protective value of *CYP2D6* is in its ability to act as a first line of defense against oxidative stress by detoxifying reactive oxygen species (ROS).[12] *CFI*, an inhibitor of the complement cascade, may work to inhibit the complement cascade; however, Aβ was shown to deleteriously interact with *CFI* causing its regulatory functions to be abolished.[18,62] In the absence of *CFI*, unregulated complement activation would take place resulting in increased inflammation.[84] Studies that support the pathways shown: 1,

Poleganov et al.[49]; 2, Yang et al.[52]; 3, Elner et al.[53] and Bian et al.[54]; 4, Wu et al.[51]; 5, Chen et al.[68]; and 6, Wang et al.[18]

Table 1

Upregulation of Differentially Expressed Genes in Aβ-Treated RPE Cells at 24 Hours

Name	Description	GenBank Accession No.	Change (*x*-Fold)	*P*
Immune response				
*IL-1β**	Homo sapiens interleukin 1, beta	NM_000576	4.80	0.0022
*RSAD2**	Homo sapiens radical S-adenosyl methionine domain containing 2	NM_080657	2.58	0.0256
*IL-8**	Homo sapiens interleukin 8	NM_000584	2.38	0.00177
LAIR1	Homo sapiens leukocyte-associated Ig-like receptor 1	NM_021706	2.32	0.0332
*MX1**	Homo sapiens myxovirus (influenza virus) resistance 1, interferon-inducible protein p78 (mouse)	NM_002462	2.18	0.0187
OAS3	Homo sapiens 2′-5′-oligoadenylate synthetase 3, 100kDa	NM_006187	1.99	0.000495
*IF144L**	Homo sapiens interferon-induced protein 44-like	NM_006820	1.98	0.00842
*IFI27**	Homo sapiens interferon, alpha-inducible protein 27	NM_005532	1.81	0.00436
OAS1	Homo sapiens 2′,5′-oligoadenylate synthetase 1, 40/46kDa	NM_002534	1.80	0.0154
PRKCZ	Homo sapiens mRNA, chromosome 1 specific transcript KIAA0505.	AB007974	1.71	0.0186
CX3CL1	Homo sapiens chemokine (C-X3-C motif) ligand 1	NM_002996	1.71	0.00906
LSP1	lymphocyte specific protein 1	W725T9	1.68	0.00255
*CXCL2**	Homo sapiens chemokine (C-X-C motif) ligand 2	NM_002089	1.68	0.023
*TNFSF10**	Homo sapiens tumor necrosis factor (ligand) superfamily, member 10 (TRAIL)	NM_003810	1.58	0.0149
OASL	Homo sapiens 2′-5′-oligoadenylate synthetase-like	NM_003733	1.57	0.016
*IL-33**	Homo sapiens chromosome 9 open reading frame 26 (NF-HEV) (C9orf26)	NM_033439	1.55	0.00679
GBP4	Homo sapiens guanylate binding protein 4	NM_052941	1.55	0.0332
MX2	Homo sapiens myxovirus (influenza virus) resistance 2 (mouse)	NM_002463	1.54	0.0191
*CFI**	Homo sapiens I factor (complement)	NM_000204	1.54	0.0234
SPN	Homo sapiens sialophorin (gpLI15, leukosialin, CD43)	NM_003123	1.50	0.0138
Apoptosis				
*XAF1**	Homo sapiens XIAP associated factor-1	NM_017523	2.10	0.0192
C8orf4	Homo sapiens chromosome 8 open reading frame 4	NM_020130	1.70	0.0152
CECR2	Homo sapiens cDNA FLJ34435 fis, clone HLUNG2000955	AK091754	1.65	0.0156
Transcription regulation				
ZNF175	Homo sapiens zinc finger protein 175	BC007778	1.92	0.00566
THC2317006	Q7IRG2(Q71RG2) FP2860, partial (26%)	THC2317006	1.89	0.0222
FOXA2	Homo sapiens forkhead box A2	NM_021784	1.76	0.0107
TEAD1	Tea domain family member 1 (SV4O transcriptional enhancement factor)	CR594735	1.75	0.0169
Transporter				
*NR4A3**	Homo sapiens nuclear RNA export factor 3	NM_022052	1.86	0.0198
C14orf68	Homo sapiens chromosome 14 open reading frame 68	NM_207117	1.68	0.00185

Name	Description	GenBank Accession No.	Change (*x*-Fold)	*P*
*SLC30A4**	Homo sapiens solute carrier family 30 (zinc transporter), member 4	NM_013309	1.64	0.0303
NPCIL1	Homo sapiens NPC1 (Niemann-Pick disease, type CI, gene)-like 1	NM_013389	1.64	0.00187
PKD2L2	Homo sapiens polycystic kidney disease 2-like 2	NM_014386	1.55	0.0118
Cell proliferation				
NPY	Homo sapiens neuropeptide Y	NM_000905	2.65	0.0252
*MT3**	Homo sapiens metallothionein 3 (growth inhibitory factor (neurotrophic))	NM_005954	1.71	0.0056
Cell signaling				
STC1	Homo sapiens stanniocalcin 1	A1476245	1.99	4.14E-05
TSHB	Homo sapiens thyroid stimulating hormone, beta	NM_000549	1.52	0.0498
Metabolism				
*CYP2D6**	Homo sapiens cytochrome P450, family 2, subfamily D, polypeptide 6	NM_000106	1.82	0.000452
SULT4A1	Homo sapiens sulfotransferase family 4A, member 1	NM_014351	2.02	0.00517
Signal transduction				
PMCH	Homo sapiens promelanin-concentrating hormone	NM_002674	1.99	0.00127
*SSTR2**	Homo sapiens somatostatin receptor 2	NM_001050	1.51	0.00651
Miscellaneous function				
EGFL8	Brain development: EGF-like-domain, multiple 8	NM_030652	1.77	0.0248
RCAN3	Calcium-mediated signaling: *RCAN* family member 3	BM457392	2.00	0.00402
PACRG	Cell death: *PARK2* co-regulated	NM_152410	1.55	0.0222
FLCN	Cell cycle: folliculin	AL831885	1.50	0.0199
*FNDC5**	Extracellular matrix: fibronectin type III domain containing 5	NM_153756	1.52	0.0299
LOC221272	Microtubule cytoskeleton organization: FLJ21659 fis, clone COL08743.	AK025312	1.64	0.0174
FLJ21272	Microtubule cytoskeleton organization: FLJ21272 fis, clone COL01753.	AK024925	1.56	0.0147
MTMR9	Phospholipid dephosphorylation: myotubularin related protein 9	AF339813	1.55	0.0394
DPP6	Proteolysis: dipeptidyl-peptidase 6	BX094874	1.54	0.0403
PMCHL2	Synaptic transmission: promelanin-concentrating hormone-like 2	NM_153381	2.36	0.00696
*HERC5**	Ubiqitin cycle: hect domain and RLD 5	NM_016323	1.73	0.000338
CLDN6	Cell-cell adhesion: claudin 6	NM_021195	1.82	0.0277
PRRG4	Calcium-ion binding: proline rich Gla (G-carboxyglutamic acid) 4 (transmembrane)	NM_024081	2.19	0.00463
SMOC1	Calcium-ion binding: SPARC related modular calcium binding 1	NM_022137	1.51	0.0104
FRMD3	Protein binding: FERM domain containing 3	BG216229	1.59	0.0138
LXN	Enzyme inhibitor: latexin	NM_020169	1.57	0.00212
CMPK2	Kinase: cytidine monophosphate(UMP-CMP) kinase 2, mitochondrial	BG547557	2.10	0.00714
TRIM14	Metal-ion binding: tripartite motif-containing 14	NM_014788	1.53	0.0141
DSCR6	Protein binding: Down syndrome critical region gene 6	NM_018962	1.87	0.0213

Name	Description	GenBank Accession No.	Change (*x*-Fold)	*P*
CI6ORF70	Protein binding: chromosome 16 open reading frame 70	BC008476	1.56	0.0419
AK123481	Protein binding: K1AA1377	AK123481	1.56	0.0034
BRD4	Protein binding: bromodomain containing 4	NM_014299	1.64	0.0341
RNASE1[*]	RNA binding: ribonuclease, RNase A family, 1 (pancreatic)	NM_198232	2.00	0.0026

The data are presented as *x*-fold changes and log-transformed *x*-fold changes. The expression level of genes greater than 1.5-fold was considered upregulated ($P < 0.05$).

[*] Genes that are selected for verification by RT-PCR.

Table 2

Downregulation of Differentially Expressed Genes in Aβ-Treated RPE Cells at 24 Hours

Name	Description	Gene Bank Accession No.	Change (*x*-Fold)	*P*
Immune response				
PSG8	Homo sapiens pregnancy specific beta-1-glycoprotein 8	NM_182707	−1.64	0.0123
SEMA4A	Homo sapiens sema domain, immunoglobulin domain (Ig), transmembrane domain (TM) and short cytoplasmic domain, (semaphorin) 4A	NM_022367	−1.75	0.00761
IL-9R	Homo sapiens interleukin 9 receptor (*IL-9R*)	NM_176786	−1.85	0.0407
Transporter				
MFSD7	major facilitator superfamily domain containing 7	NM_032219	−1.52	0.0141
SLC12A3	Homo sapiens solute carrier family 12 (sodium/chloride transporter), member 3	NM_000339	−1.59	0.0158
TRPV5	Home sapiens transient receptor potential cation channel, subfamily V, member 5	NM_019841	−1.61	0.0367
GLTPD1	glycolipid transfer protein domain containing 1	NM_001029885	−1.64	0.00111
ACCN1	Homo sapiens amiloride-sensitive cation channel 1, neuronal (degenerin)	NM_183377	−1.69	0.00179
Metabolism				
LYZL2	Homo sapiens lysozyme-like 2	NM_183058	−1.49	0.0139
ALDH1L1	Homo sapiens aldehyde dehydrogenase 1 family, member L1	NM_012190	−2.04	0.00838
Transcription regulation				
MAFA	Homo sapiens v-maf musculoaponeurotic fibrosarcoma oncogene homolog A	NM_201589	−1.56	0.00821
FOXE1	Homo sapiens *HFKH4* mRNA for fork head like protein	X94553	−1.64	0.0499
Miscellaneous function				
RNF36	Apoptosis: ring finger protein 36	NM_182985	−1.61	0.0192
*THBS1**	Cell motility: Thrombospondin 1	N48043	−1.64	0.000305
ACTL6B	Cytoskeleton: actin-like 6B	NM_016188	−2.22	0.00128
PLCXD2	Intracellular signaling cascade: phosphatidylinositol-specific phospholipase C, X domain containing 2	NM_153268	−1.52	0.0137
MASTL	Protein phoshorylation: microtubule associated serine/ threonine kinase-like	THC2405366	−1.56	0.0208
GPR78	Signal transduction: G protein-coupled receptor 78	NM_080819	−1.69	0.000824
FIBIN	Translation initiation factor: fin bud initiation factor	NM_203371	−1.52	0.00345
RSPO3	Wnt receptor signaling: R-spondin 3 homolog (Xenopus laevis)	NM_032784	−1.96	0.00811
ACPP	Acid phosphatase activity: acid phosphatase, prostate	NM_001099	−1.64	0.0189
PLEKHA3	Phospholipid binding: pleckstrin homology domain containing, family A (phosphoinositide binding specific) member 3	BC035471	−1.64	0.000975

The data are presented as *x*-fold changes and log-transformed *x*-fold changes. Decreased expression changes are expressed as −(treatment/ control)$^{-1}$. The expression levels of genes decreased more than −1.5-fold are considered downregulated ($P < 0.05$).

* Genes that are selected for verification by RT-PCR.

Table 3

RT-PCR Primers

Gene	Forward Primer	Reverse Primer	Reference
IL-8	AGGTGCAGTTTTGCCAAGGA	TTTCTGTGTTGGCGCAGTGT	
IL-1β	AAGCTGAGGAAGATGCTG	ATCTACACTCTCCAGCTG	
CFI	ATTGTGGAGACCAAAGTGATGAAC	TGATACTGGCTTGGAATGCAAA	
CXCL2	GATAGAGGCTGAGGAATCCAAGAA	ACATTTCCCTGCCGTCACA	
RSAD2	ACACAGGAATAATGACCCCAAAA	TGAGCTAAATGTCAGGTCCTGTGTA	
MX1	GCCAGGACCAGGTATACAG	GCCTGCGTCAGCCGTGC	Leong et al.[32]
IFI44L	CCAATTACACCTGAGCATTCTACTTTT	AGACATAAGCCACACAGTGAATCCT	
IFI27	TGGCTCTGCCGTAGTTTTGC	CACAGCCACAACTCCTCCAAT	
HERC5	GGGATGAAAGTGCTGAGGAG	CATTTTCTGAAGCGTCCACA	Kroismayr et al.[33]
SLC30A4	GGCTATCATCAAAATCACCAACCA	CGGTGATGAGCATTATATCTCCATT	Overbeck et al.[34]
IL-33	CACCCTCAAATGAATCAGG	GGAGCTCCACAGAGTGTTCC	Carriere et al.[35]
THSD2	TGCACGAAGAAGGGAAAAACAT	TCTCGGACCCGTGTTTCAG	
TNFSF10	ATGGCTATGATGGAGGTCCAG	TTGTCCTGCATCTGCTTCAGC	Komatsuda et al.[36]
XAF1	CCAGAAAATAAGTATTTCCACC	TTATACTTCTTGTCTTTGGACG	Kempkensteffen et al.[37]
CYP2D6	CCTACGCTTCCAAAAGGCTTT	AGAGAACAGGTCAGCCACCACT	Kojima et al.[38]
SSTR2	CCCCAGCCCTTAAAGGCATGT	GGTCTCCATTGAGGAGGGTCC	Kumar et al.[39]
NR4A3	CAACTAGTCCAACCCCTTAAAATTCA	ACCTTGAGIAACTCTTCACCCTTCA	
FN	GACCACACCGCCCACAAC	TCCTACATTCGGCGGGTATG	
GAPDH	CATCCATGACAACTTTGGTATCGT	CAGTCTTCTGGGTGGCAGTGA	Wang et al.[25]

In total, 18 genes were selected for validation by RT-PCR. Nearly, all expression patterns were comparable to the microarray data.

Table 4

Summary of GSEA Analysis

	Gene Set(Pathway)	Genes within Gene Set (Top 20 only)	NES	FDR
1	DAC_BLADDER_UP(IFN signaling)	*OAS2, MX1, IF144L, OAS1, CXCL2, TNFSF10, STC1, IFIT3, STAT1, ICAM1, MMP1, IRF7, CIS, MX2, C3, IL13RA2, TNFAIP3, HBEGF, NT5E, SLP1*	2.38	0.000
2	IFNA_UV-CMV_COMMON_HCMV_6HRS_UP (IFN and inflammatory signaling pathways)	*OAS2, RSAD2, MX1, IFI44L, OAS1, IF127, OASL, TNFSF10, IFIT3, INDO, ISG20, CIORF38, TDRD7, STXI1, BAZIA, SAMHD1, TLR3, IRF7, GCH1, MX2*	2.37	0.000
3	DAC_IFN_BLADDER_UP (IFN signaling)	*OAS2, MX1, OAS1, CXCL2, TNFSF10, IFIT3, STAT1, ICAM1, IRF7, CIS, MX2, C3, ILI3RA2, TNFAIP3, SLP1, CCL5, CCL20*	2.36	0.000
4	TAKEDA_NUP8_HOXA9_3D_UP (IFN signaling)	*OAS2, RSAD2, MX1, IFI44L, OAS3, OAS1, CTSG, HERC5, IF127, OASL, IFIT3, IFIT1, IFIT2, IFIH1, CCL18, INDO, PLSCR1, DDX58, EPSTI1, DST*	2.35	0.000
5	IFNA_HCMV_6HRS_UP (IFN and inflammatory signaling pathways)	*OAS2, RSAD2, MX1, 1F144L, OAS1, IF127, OASL, TNFSF10, IFIT3, INDO, PLSCR1, ISG20, STAT1, TRIM22, IFIT5, CIORF38, TDRD7, STXI1, ZBTB20, BAZIA*	2.32	0.000
6	CMV_HCMV_TIMECOURSE_12HRS_UP (IFN and inflammatory signaling_pathways)	*OAS2, RSAD2, MX1, OAS1, OASL, TNFSF10, IFIT3, ISG20, CH25H, B4GALT5, IRF7, SOD2, PRPF19, MX2, GBP2, TNFAIP6, RARRES3, RHOB, CCL5, NR4A3*	2.28	0.000
7	TAKEDA_NUP8_HOXA9_8D_UP (IFN signaling)	*OAS2, RSAD2, MX1, IFI44L, OAS3, OAS1, CTSG, HERC5, IFI27, LXN, NR4A2, IFIT3, IFIT1, IFIT2, DHRS3, C20ORF103, IFIH1, MTSS1, INDO, DDX58*	2.18	0.001
8	BENNETT_SLE_UP (IFN signaling)	*OAS2, MX1, IFI44L, OAS1, OASL, TNFSF10, IFIT3, PLSCR1, CAMP, STAT1, C2, TAP1, IFI35, TDRD7, IFITM3, IRF7, APOBEC3C, MX2, SERPING1, LY6E*	2.14	0.002
9	TAKEDA_NUP8_HOXA9_10D_UP (IFN signaling)	*OAS2, RSAD2, MX1, IFI44L, OAS3, OAS1, HERC5, DCAL1, IFI27, OASL, NR4A2, IFIT3, IFIT1, IFIT2, DHRS3, CD38, C20ORF103, IFIH1, INDO, DDX58*	2.12	0.003
10	IFNALPHA_NL_UP (IFN signaling)	*RSAD2, MX1, IFI44L, IF127, TNFSF10, PLSCR1, VCAM1, STAT1, IFITM1, UBE2D3, BST2, IRF7, CALR, MX2, HLA-E, PIAS4, KIAA0409, UBE2L6, AKR7A2, PSME1*	2.10	0.004
11	SANA_TNFA_ENDOTHELIAL_UP (IFN, inflammatory, and immune signaling pathways)	*IL8, OAS2, MX1, IFI44L, OAS3, OAS1, CXCL2, CX3CL1, IFIT1, CXCL3, IFIH1, FIJ20035, PARP14, VCAM1, BIRC3, UBD, CCL2, GBP1, OXR1, NFKBIA*	2.07	0.006
12	SANA_IFNG_ENDOTHELIAL_UP (IFN, inflammatory, and immune signaling pathways)	*OAS2, MX1, IFI44L, QAS1, TNFSF10, CX3CL1, NOD27, IFIH1, INDO, ILI8BP, FLJ20035, PARP14, TNCRNA, STAT1, UBD, DTX3L, GBP1, LAP3, C17ORF27, CXCL9*	2.04	0.008
13	NTHIPATHWAY (NF-κB signaling-related to inflammation)	*ILIB, IL8, DUSP1, NFKBIA, NR3C1, EP300, CREBBP, TGFBR1, IKBKB, MAP2K6, TLR2, RELA, MAPK14, MAPK11, TGFBR2, CHUK, MAP3K7, NFKB1, MYD88, MAP2K3*	2.04	0.008
14	GALINDO_ACT_UP (Inflammatory and apoptosis signaling)	*IL1B, CXCL2, ILI8RAP, ILIRN, PTGS2, PDGFB, LILRB4, DUSP1, NFKB1A, IER3, FOSL1, CSF3, ICAM1, CCL3, RREB1, TNFSF9, BCL3, UBC, TNFAIP2, CCL4*	2.04	0.008
15	CMV_UV-CMV_COMMON_HCMV_6HRS_UP (IFN and inflammatory signaling)	*RSAD2, MX1, OASL, NR4A2, IFIT3, ILI1, ZC3HAV1, RIPK1, PMAIP1, POLG2, ATF3, CREM, GCH1, C12ORF22, PSCD1, NR4A3, BTRC, SLC745, NR4A1*	2.03	0.007

GSEA analysis of the microarray results for Aβ treatment versus control helped in identifying gene sets correlated predominately with inflammation. Pathway 13, NTHIPATHWAY is identified as one of the inflammatory gene sets of particular interest, such as *IL-β* and *IL-8*, the top-ranked genes in this set. All gene sets can be accessed at the Molecular Signatures Database, http://www.broad.mit.edu/gsea/msigdb/index.jsp (provided in the public domain by the Broad Institute at Massachusetts Institute of Technology, Cambridge, MA).

Table 5

Associated Gene Found in the NTHIPATHWAY Gene Set

	Probe	Rank in Gene List	Rank Metric Score	Running Es	Core Enrichment
1	*ILIB**	0	3.264	0.3542	Yes
2	*IL8**	8	2.035	0.5747	Yes
3	*DUSP1*	961	0.461	0.5703	Yes
4	*NFKBIA*	1,052	0.439	0.6128	Yes
5	*NR3C1*	1,116	0.428	0.6556	Yes
6	*EF300*	1,747	0.320	0.6543	Yes
7	*CREBBP*	1,812	0.311	0.6844	Yes
8	*TGFBR1*	2,068	0.279	0.7002	Yes
9	*IKBKB*	3,348	0.180	0.6466	No
10	*MAP2K6*	3,627	0.165	0.6486	No
11	*TLR2*	4,454	0.126	0.6151	No
12	*RELA*	4,626	0.119	9.6182	No
13	*MAPK14*	5,538	0.082	0.5750	No
14	*MAPK11*	5,719	0.075	0.5729	No
15	*TGFBR2*	6,135	0.058	0.5554	No
16	*CHUK*	6,171	0.057	0.5596	No
17	*MAP3K7*	6,989	0.029	0.5160	No
18	*NFKB1*	7,241	0.020	0.5039	No
19	*MYD88*	8,062	−0.006	0.4576	No
20	*MAP2K3*	10,744	−0.094	0.3146	No
21	*MAP3K14*	12,052	−0.142	0.2553	No
22	*TNF*	16,472	−0.524	0.0597	No

A detailed look into this gene set shows that *IL-1b* and *IL-8* are the top-ranked genes in our experimental Aβ dataset. Genes that are found in the leading edge of this gene set are marked “Yes”in the core enrichment column. They are the genes that significantly contribute to the total enrichment score of the NTHIPATHWAY gene set.